STATISTICAL ANALYSIS OF DESTRUCTIVE SATELLITE RE-ENTRY UNCERTAINTIES

B. Karahan[1,2], **M. Papa**[2], **D. Galla**[3], **M. Fugmann**[3], **S. Klinkner**[3]

[1] *University of Stuttgart, Stuttgart, Germany, Email: bahar.karahan@ksat-stuttgart.de*
[2] *European Space Agency, Clean Space Office, ESTEC, Noordwijk, The Netherlands*
[3] *Institute of Space Systems, University of Stuttgart, Stuttgart, Germany*

ABSTRACT

With the growth of orbital debris and rising satellite launch traffic, the number of objects re-entering Earth's atmosphere increases.
Ensuring the complete demise of satellites during uncontrolled re-entry is critical to minimize the casualty risk to populations and infrastructure on the ground. To address these challenges, ESA missions adhere to space debris mitigation requirements, which limit the on-ground casualty risk of uncontrolled re-entry to 10^{-4}.
Uncertainties for re-entry simulation of spacecraft have to be taken into account. Leveraging ESA's Debris Risk Assessment and Mitigation Analysis (DRAMA) Survival And Risk Analysis (SARA) software toolchain with the pyDRAMA extension, satellite components within the Stuttgart Operated University Research CubeSat for Evaluation and Education (SOURCE) satellite, were modelled to evaluate their behaviour during re-entry. Uncertainties, such as those related to environmental conditions and material properties, were applied as outlined in the ESA Demise Verification Guidelines (DIVE) document [4, 12, 36].
By conducting Monte Carlo (MC) simulations, this study reports on how uncertainties affect predictions of break-up and demise.

Keywords: Demise; Uncertainties; Uncontrolled re-entry.

1. INTRODUCTION

The space sector is reaching a new phase of industrial development [29]. Satellites have become a commercial asset. The growing density of space objects and debris, driven by intensified space activities such as mega-constellations of hundreds or thousands of satellites and growing accessibility to space through commercialisation and ride-share opportunities by launchers, threaten access to space, and Earth [22].
Due to this increase, nationwide warning services will more frequently issue warnings about space debris from low Earth orbit (LEO). The casualty risk for human populations, infrastructures, and aviation is increasing due to the growing number of objects re-entering the Earth's atmosphere and an increasing population [17, 25, 34]. Therefore, as a requirement, all ESA missions must ensure a casualty risk of less than 1 in 10 000 in case of uncontrolled re-entry [13]. For 2025, the forecast predicts a total of 646 debris objects re-entering Earth's atmosphere, assuming no additional objects are introduced into the space environment [18]. Of these, 444 are Starlink satellites with a total mass of 152 t, and 65 are rocket bodies with a total mass of 113 t [18].
When the spacecraft re-enters, it faces aerothermal and mechanical loads, which break-up the satellite [15]. It is only a matter of time until people are injured or killed by debris. Ground impacts to human-populated areas will become more frequent as critical components such as reaction wheels, tanks, and optical payloads can survive the atmospheric re-entry [12, 4]. The United Nations Office of Outer Space Affairs (UNOOSA) Liability Convention Article II states that *"A launching State shall be absolutely liable to pay compensation for damage caused by its space object on the surface of the Earth or to aircraft flight"* [38]. Risk assessment tools such as DRAMA or SCARAB should be used to assess the damage that a spacecraft can cause. Uncertainties during the modelling and the destructive re-entry process should be considered and addressed while assessing the casualty risk of a spacecraft to verify whether the spacecraft complies with Space Debris Mitigation requirements and does not cause harm by re-entering [8]. To account for uncertainties, Monte Carlo (MC) simulations should be conducted [16]. In this regard, this study aims to determine through analysis, using the CubeSat SOURCE, how defined uncertainties impact the simulation's results.

2. FUNDAMENTALS

2.1. Re-entry process

Unlike controlled re-entries, which involve steep trajectories and high heat fluxes over a short period, uncontrolled

Proc. 9th European Conference on Space Debris, Bonn, Germany, 1–4 April 2025, published by the ESA Space Debris Office
Editors: S. Lemmens, T. Flohrer & F. Schmitz, (http://conference.sdo.esoc.esa.int, April 2025)

re-entries typically follow trajectories with shallow flight path angles (FPA) up to $-2°$ [31].
A shallow re-entry trajectory leads to extended atmospheric interaction, allowing the spacecraft to absorb a higher integral heat load, causing wider ground fragment dispersion [31]. An overview of the main re-entry and its processes is given in Fig. 1, indicating their driving parameters such as heat flux, mechanical loads and flow effects during the atmospheric re-entry [12].

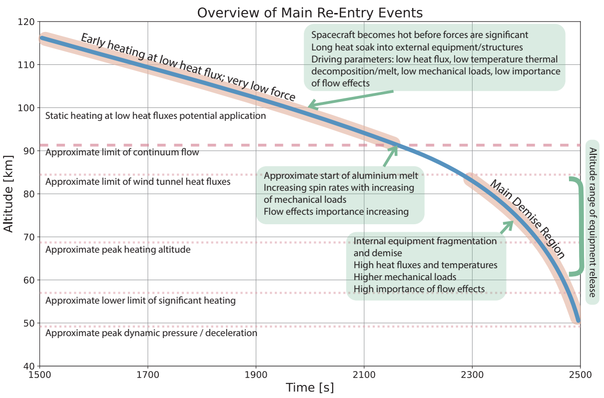

Figure 1: Overview of main re-entry events within a standard re-entry trajectory, where the blue line is the trajectories' altitude over time, with specific event thresholds indicated with dotted lines [12]

.

All re-entering spacecraft are exposed to the effects of the atmosphere. Atmospheric models enable the calculation of a spacecraft's destruction and casualty risk. The static atmospheric model used in the DRAMA SARA module as default is the commonly used US Standard Atmosphere 1976, which provides static atmospheric properties such as temperature up to an altitude of $150\,\mathrm{km}$ [26, 35]. It represents the gas composition, density and temperature profiles [36].
During re-entry, spacecraft components are exposed to heat loads, pressure, and density of the atmospheric layers [26]. The main break-up event occurs between $76\,\mathrm{km}$ to $90\,\mathrm{km}$ with a peak at $83\,\mathrm{km}$ in the mesosphere, which begins at $50\,\mathrm{km}$ and reaches $85\,\mathrm{km}$ altitude, since the air density is sufficiently large to burn up objects re-entering [12, 33]. From $85\,\mathrm{km}$ to $600\,\mathrm{km}$, the temperature curve increases drastically within the thermosphere [12, 33]. While the temperatures in these heights are relatively high, the pressure is extremely low, below $1\,\mathrm{mPa}$, resulting in low heat flux [33]. The spacecraft begins to experience initial aerothermodynamic effects in this altitude range.
Earth's rotation, solar activity, and solar wind influence atmospheric density and, thus, behaviour during demise. Overall, the demise process occurs in the meso- and thermosphere between $120\,\mathrm{km}$ to $30\,\mathrm{km}$ and the peak heat flux is $200\,\mathrm{kW\,m^{-2}}$ to $600\,\mathrm{kW\,m^{-2}}$ [31].

2.2. Radiative Equilibrium

Heat is transferred from objects with high temperatures to objects with low temperatures. In the case of re-entry, the thermal response of the object combines heat storage and heat loss due to radiation from the surface of the component [21]. As soon as the heat flux into one object equals the radiative heat loss through the object's surface, radiative equilibrium is reached [21]. The following Eq. 1 gives further understanding:

$$\dot{q}_{\text{aero}} = \sigma \cdot \varepsilon \cdot T^4_{\text{W,RE}}. \tag{1}$$

In the Eq. 1 $\dot{q}_{\text{aero}}$ is the heat flux entering the object, σ represents the Stefan-Boltzmann constant, ε represents the emission coefficient, and $T_{\text{w,RE}}$ is the wall temperature at the radiative equilibrium.

2.3. Ballistic coefficient

Another parameter that influences the survivability of a component is its ballistic coefficient (BC) [32]. The BC is calculated as given in Eq. 2:

$$BC = \frac{M}{C_d \cdot A}. \tag{2}$$

It is, therefore, dependent on the drag coefficient C_d, the cross-section A of the component and its mass M. The BC directly influences the velocity and the trajectory of the component during re-entry, as well as the aerodynamic forces it experiences. A higher BC typically results in a faster re-entry and a higher peak heating while the integral heating remains low due to shorter exposure. In contrast, a lower BC often leads to slower descent, prolonged exposure, and potentially higher localised heating rates. However, low BCs may cause rapid deceleration to speeds where heat flux becomes sufficiently low, reducing the total heat load despite longer exposure durations. The Eq. 3 outlines the relation of the BC to the impact velocity v_i on ground

$$v_i = \sqrt{\frac{2 \cdot BC \cdot g_0}{\rho_0}}. \tag{3}$$

where ρ_0 is the atmospheric density at sea level. The impact velocity is used to calculate the kinetic energy upon impact and verify whether the $15\,\mathrm{J}$ threshold is reached. The heating rate of the component is, therefore, not only influenced by the material properties but also by the velocity during re-entry, which is dependent on the BC and, thus, the components' dimensions and mass. For example, components with a low BC, such as solar arrays, are more likely to demise during re-entry due to higher drag forces and greater heat dissipation.

2.4. Critical Components

The main drivers for a component's demisability are the material, with its melting temperature, the geometry, the dimension, and where the components are located in the spacecraft. While panels located on the outside of the spacecraft are directly exposed to the thermal and mechanical loads of a re-entry, components located in a parent component, such as optics, lenses and tanks, will face these loads in a later stage, as components contained in other parent components will be released upon the break-up or demise of the parent component [32].
ESA established a material database: Material Demisability Database (ESTIMATE), that can be used to replicate material behaviour upon demise. It characterises material properties with, for example, conducted Plasma Wind Tunnel (PWT) tests within demise studies [14, 20, 27]. Critical components of the CubeSat SOURCE were identified through PWT observations in the facility PWK1 of the IRS [1, 8]. The IRAS Sandwich structure with a PEEK honeycomb core, the payload printed circuit board (PCB), the MeSHCam with its lenses, the magnetorquers the titanium rods and the battery were identified as critical components [1].

3. UNCERTAINTIES DURING THE RE-ENTRY

While uncontrolled re-entry is simpler to implement than controlled re-entry, its safety relies on probability. As outlined in the guidelines, knowing what effects uncertainties can have during destructive re-entry is crucial. Requirements must be statistically validated to account for existing uncertainties [12]. This is also explicitly stated in the ESA Re-entry Safety Requirements, which notes: *"Analysis methodology and assumptions for the re-entry casualty risk analysis of the space system, or re-entering elements thereof, shall include: Safety margins and probability distribution functions or dispersions for the input parameters of the re-entry modelling to cover their uncertainties."* [16]. An overview of the statistical uncertainties applied is given in the Tab. 1 below [4, 8, 12, 36].

Table 1: Defined uncertainty parameters [12, 36]

Parameter [12]	Range/Distribution [12]
Aerodynamic drag (Continuum)	$\pm$10% uniform (local) and normal (global)
Heat Flux (Continuum)	$\pm$30% uniform (local) and normal (global)
Oxidised Emissivity	$\pm$25%, triangular
Specific heat capacity	$\pm$5% normal (3-σ limit)
Latent heat	$\pm$5% normal (3-σ limit)
Alloy melting temperature	$\pm$30K uniform

It shall be mentioned that this is just a selection of uncertainties, as more uncertainties are present. Additional uncertainties exist but could not be implemented in DRAMA and require advanced tools like SCARAB, or were simply not necessary, as the DRAMA model of SOURCE does not include joints that would trigger a break-up upon reaching a certain altitude or temperature [12]. Mass and material uncertainties shall be applied to cover uncertainties from modelling and assumptions made during modelling [27]. Additionally, uncertainties regarding atmospheric properties shall be applied [35]. Whilst the local heat flux and drag uncertainty are applied uniformly to each component individually, a global uncertainty is applied with a normal distribution to all components due to uncertainty in the density from the atmospheric model.

3.1. DRAMA

Demise modelling tools are required to assess spacecraft demisability and verify compliance with space debris mitigation guidelines [19]. The demisability of a spacecraft can determine whether it requires a controlled, semi-controlled, or uncontrolled re-entry strategy or implementation of D4D technologies [19]. Conducting such assessments early in the spacecraft design phase can prevent critical design changes later [39]. One such tool is the DRAMA SARA suite, consisting of two modules: the Spacecraft Entry Survival Analysis Module (SESAM) and the Spacecraft Entry Risk Analysis Module (SERAM). These modules allow predicting a spacecraft or component's survivability and associated casualty risks [19].

4. METHODOLOGY

4.1. Modelling SOURCE

The CubeSat was modelled with components summing up to a mass of $4.42\,\mathrm{kg}$ as stated in the space debris mitigation report of SOURCE [7]. Recent measurements determined that SOURCE has a mass of $4.45\,\mathrm{kg}$. Given the possibilities of DRAMA modelling, the model is a simplified version of the satellite.
All important components were modelled conservatively, ensuring that the components do not survive in reality due to liberal modelling choices if the component itself could not be originally represented given the simplicity of the shapes. The component's dimensions were modelled using the most recent Computer-Aided Design (CAD) files or datasheets available shown in Fig. 2. All component masses were derived from tables, and other simulation data that was available. Masses from different sources were incongruent, so decisions needed to be made to fit the end mass.

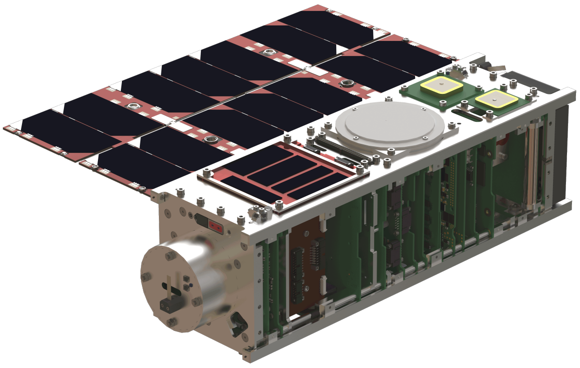

Figure 2: SOURCE rendering of an isometric perspective illustrating the CubeSat's components, with the side panel and solar panel removed on one side to provide a detailed view of the internal structure [30].

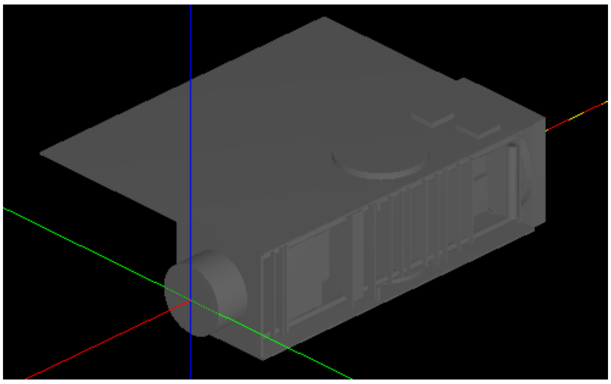

Figure 3: SOURCE DRAMA SARA model with an isometric perspective illustrating the CubeSat's components, with the side panel and solar panel removed on one side to provide a detailed view of the internal structure.

Besides the mass and dimension, that define the BC, each component primitive is modelled with one material of a monolithic nature. These materials originate from the ESTIMATE database and are already included in DRAMA. SOURCE's final total mass and dimension align with the latest CAD files and former simulation inputs. For simplifications, harness and smaller components such as sensors, screws and bolts were not modelled, as they are also not considered as critical compared to other components within SOURCE, such as the titanium rods. The battery cells were modelled with the drama-A316 steel material instead of the drama-Bat-Li material, also the PCBs were modelled with the drama-AA7075 material instead of the drama-el-mat material [24]. According to experts, the material models for lithium batteries and electrical material do not represent the demise behaviour well enough [24].
The materials are derived based on test data from PWT tests. That is why some materials might be outdated as technology evolves. New and more representative materials will be available in the new ESTIMATE update. All aluminium parts were modelled as drama-AA-7075, and the camera lenses as drama-SiC. The IRAS sandwich was modelled with the drama-HC-CFRP-4ply material for its face sheets, and the drama-HC-AA7075 as a PEEK material for honeycomb structures does not exist. SOURCE will reenter uncontrolled from a decaying SSO orbit. The parameters chosen for the simulation in Tab. 2 are based on previous studies done with SCARAB [6, 37].

Table 2: Cartesian ECI J2000 coordinates for position and velocity transformed from the Keplerian elements (J2000).

Parameter	Value	Unit
Position x	4984.48	km
Position y	3993.19	km
Position z	1116.49	km
Velocity x	-0.40	$\mathrm{km\,s^{-1}}$
Velocity y	-1.64	$\mathrm{km\,s^{-1}}$
Velocity z	7.66	$\mathrm{km\,s^{-1}}$

4.2. Uncertainties by Modelling

The modelling of a spacecraft heavily depends on the engineer taking care of the simulations. As such, modelling decisions are made based on their experience and expertise. Therefore, adhering to established modelling guidelines is essential, such as the DRAMA SARA modelling document or the DIVE document [4, 12].
To ensure accuracy, it is crucial to have a single source of truth for the dimensions and masses of the components, along with an up-to-date database of data sheets. Such a single source of truth database also saves the engineer modelling time. Data sheets can provide valuable information regarding dimensions, mass, and materials.
However, this study has observed that companies may not respond to specific requests or withhold information essential for creating a representative model of specific components. This was the case in this study for the MeshCam, the transceiver and the antenna.
However, spacecraft contain materials that are not listed in the ESTIMATE database. Therefore, using a material which might approximate the expected demise behaviour brings considerable uncertainty into play [4].

4.3. Simulation

Running the standard DRAMA simulation with the GUI, the altitude and the demise points of the components are given as an output shown in Fig. 4 It can be seen that most components demise at an altitude between $80\,\mathrm{km}$-$90\,\mathrm{km}$. Even though previous tests show that some parts survive, they are under the $15\,\mathrm{J}$ threshold, and therefore, the simulation stops taking them into account and marks them as uncritical. No casualty risk was computed as SOURCE is a CubeSat under $5\,\mathrm{kg}$.
However, this simulation does not account for uncertainties.

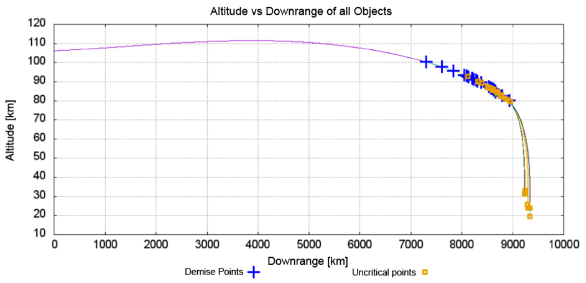

Figure 4: Altitude vs downrange of all components showing demise and uncritical points. The altitude and the downrange in km are shown for the re-entry trajectory. While the blue crosses mark the demise points of different components, the yellow rectangles mark uncritical points of components reaching a 15 J threshold.

4.4. Toolchain

To account for uncertainties, a conventional MC simulation was conducted [4]. The minimum number of 2000 runs is recommended by the modelling guidelines [4]. To ensure the required 2000 runs were achieved despite potential crashes of the DRAMA software, a total of 2500 runs were executed for each uncertainty. This is a highly conservative threshold, as typically only 100 to 200 runs failed, ensuring the 2000-run requirement was comfortably met.
With the pyDRAMA extension, the user can use Python 3 to create scripts that interact with the DRAMA software [10, 11]. In the scope of this study, a toolchain that conducts a MC simulation was evaluated, improved and executed to account for uncertainties and see their effects on the different components of SOURCE [28].
To execute the simulation, two scripts are needed:
one main script and a helper script that generates the randomised scaling factors and applies them to the different parameters. Fig. 5 shows this tool chain's workflow.
The toolchain was set up in a Linux environment using a virtual machine. DRAMA 3.1.0 and the Python extension are needed, and input and output folders are necessary for the scripts to work properly. The project, which is the SOURCE model created with the DRAMA GUI, is exported as a zip file (source.dpz) and put into the input folder. This project contains all the necessary configuration data that is later adapted by the scripts.
Once the main script is executed, the output directory is created. It calls functions from the helper script that create several randomised scaling factors and applies them to the spacecraft's initial conditions and its material properties that are saved in XML files contained in the zip file. These inputs are then compiled so that SARA can read these inputs. Finally, casualty risk results are parsed. However, this was not possible in the case of SOURCE, which has no casualty risk in most of the runs. Eexecuting the script with a larger platform ensures that components survive upon re-entry with kinetic energy over 15 J calculates the overall casualty risk.
The effect of the uncertainties is shown by analysing the aerothermal text files that list important data about the object's demise throughout the altitude. The data is plotted using an external script that reads the data. The helper script generates random samples from distributions for input parameters (e.g., drag, heat flux, and material properties) using basic MC sampling by drawing from standard distributions (uniform, normal, triangular). Each run represents one possible scenario based on the randomly perturbed inputs, and all simulations are conducted independently.

4.5. Parameter Randomisation for Drag, Heat Flux, and Mass Uncertainties: randomise_model

The physical properties of the spacecraft are randomised using scaling factors that affect the mission's drag coefficients, heat flux, and mass.
The uncertainty range is specified in the function parameters for each uncertainty. The specific range and distribution type are taken from documents like DIVE and are further specified in Tab. 1.
The table accounts for drag coefficient and heat flux uncertainties. However, in the script, these uncertainties are implemented twice, once globally and once individually for each component. The global uncertainty accounts for uncertainties in atmospheric properties such as density, which affect all components similarly. The individual uncertainty, on the other hand, reflects differences in shape, orientation, and geometry between components, which cause each to experience local variations in drag and heating. The global drag factor applies changes with a range of 10 % and a normal distribution while the local drag uncertainty is applied uniformly. The same applies to the heat flux, where the uncertainty range is 30 %.
The mass is normally distributed with a 20 % range. All uncertainties are stored in an external uncertainties.csv file to be able to conduct a sensitivity analysis and trace back which run used which uncertainties.

4.6. Material Property Randomisation: randomise_project_xml

This function applies material uncertainties to the material properties specified in the material.xml of the project. Important to mention is that the material directory path must be adapted to the location of the XML file of the materials defined within the project file (in this case, source.dpz), as the name changes from project to project and individually added materials within the project are listed within this XML data frame.
The default number of materials is 21, and each material is assigned to a number. If the user adds custom materials, this number changes and additional entries are listed in the XML file, which may be important when handling the material.xml file for result processing. This function dynamically scales the properties without being hard-coded, ensuring proper handling of the scaling process as material uncertainties were not applied in the previous code.

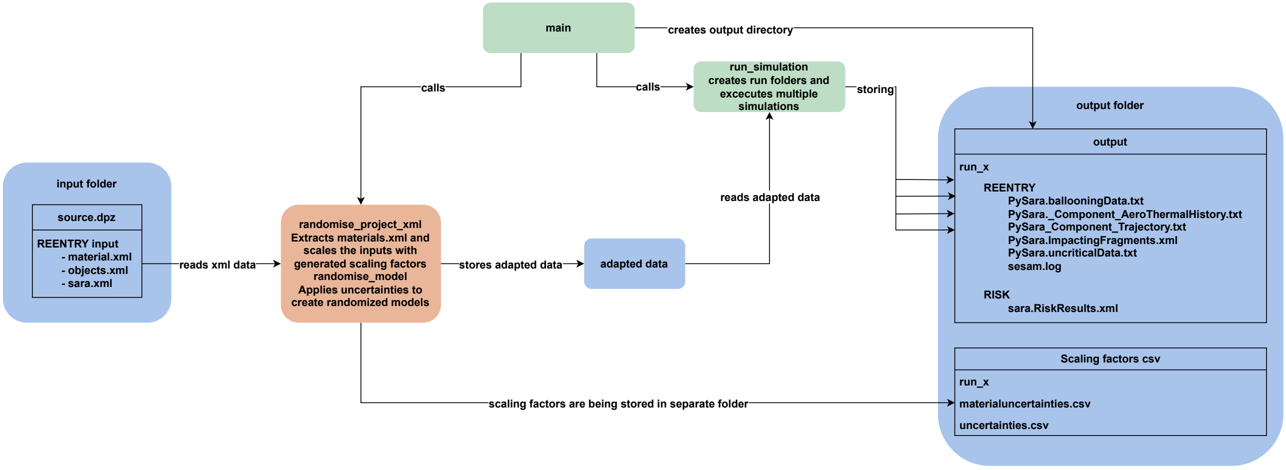

Figure 5: Workflow of helper and main script. The main script (indicated in green) calls the functions of the helper script (orange), which generates and applies the model and material scaling factors to the source.dpz XML documents. The adapted data is saved, so the main simulation function can use it to generate the different simulation outcomes into the different run folders. The helper script outputs the scaling factors into CSV documents that can be used to conduct a sensitivity analysis. The output files are the aerothermal files, Gnuplot files, trajectory files and information about the impacting fragments. If there are impacting fragments, a risk folder for this run will be generated by SERAM.

The code only applies the scaling factors to materials tagged as *"metalMaterial"* in the XML. To account for the alloy melting temperature uncertainty, an offset of ±30K to the initial temperature with a uniform distribution was applied.
A scaling factor for the oxidised emissivity is applied with a range of 25 %, following a triangular distribution. The material's heat capacity is subject to uncertainties within a range of 5 %, corresponding to a $3-\sigma$ limit. The latent heat required to melt the material is scaled using a normal distribution, with an uncertainty range of 5 %, corresponding to a $3-\sigma$ limit. The material scaling factors are stored in an external material_uncertainties.csv file [12].

5. RESULTS

Scatter plots were generated by varying one uncertainty input parameter at a time, showcasing the distribution of the demise points with colour variation. The accumulation is represented by histograms divided into different mass categories. The scaling factors and offsets for the uncertainties in heat flux, drag, mass, latent heat of melting, alloy melting temperature, heat capacity, and oxidised emissivity are applied along the x-axis of the plot, while the relevant final altitudes are represented in the y-direction. These final altitudes provide insight into the demise behaviour of the component. The distribution of both the input parameters and the final altitude computed by DRAMA is illustrated to specifically see the areas of the highest density of the number of final altitudes.
The final altitude is divided into three different colours using 3D colouring to give the plot an additional dimension to understand the demise behaviour further.
The three categories are:

- Component demises completely with an end mass of 0 kg: blue
- Component demises not completely with an end mass of >0 kg: orange
- Component does not demise, and the end mass equals the initial release mass: green

DRAMA stops computing the re-entry analysis for components that either fully demise or fall below the kinetic energy threshold of 15 J. As a result, a component's final mass can be either approximately 0 kg or greater. If the last mass and the last altitude computed by the simulation are greater than 0 kg and 0 km, respectively, this indicates that the computed kinetic energy was below 15 J.

Table 3: Results of selected components without any uncertainties applied. Mass values are colour-coded to indicate if they are equal to 0 kg or slightly above.

Object	**Last Mass** [kg]	**Last Altitude** [km]
Battery Cell	0.0	79.74
Payload PCB	0.0	90.26
Titanium Rod	0.0	82.08
S-Band Antenna	0.0	86.49
Solar Panel	0.0	98.19
Spacer	0.0	84.29
IRAS Face Sheet	0.0	90.78
MGT Core	0.0	81.22
Lens	0.004	19.35
IRAS Honeycomb	0.0	91.3

5.1. Uncertainties and their Effects

The following section discusses the sensitivity analysis conducted for each element and uncertainty. Data taken into account for discussion are the final altitudes, as SOURCE did not generate enough risks to conduct a statistical analysis. Instead, the final altitudes at which the component demises or gets uncritical is observed. To discuss the data in detail, this study presents a combination of full-scale plots covering the entire re-entry process, from the release altitude down to ground level, as well as zoomed-in plots. Given that some deviations are minimal, a zoomed-in view enhances the visibility of trends. This overall approach allows us to get immediate visual comparability across different uncertainties applied. The demise altitudes remain directly comparable via the y-axis values provided. The plots shown will be reduced to the minimum of necessary plots, as the plots within one uncertainty often show similar behaviour.

Heat Flux:
The heat flux variation affects the final altitude in a way that the more heat flux is applied, the closer the component demises to its original release altitude, showing a saturation curve structure of the scatter plot as in Fig. 6. The demise at the scaling factor around factor 1 aligns with the standard DRAMA run with no uncertainties applied. Due to the normal distribution, the densest area is around the scaling factor 1.

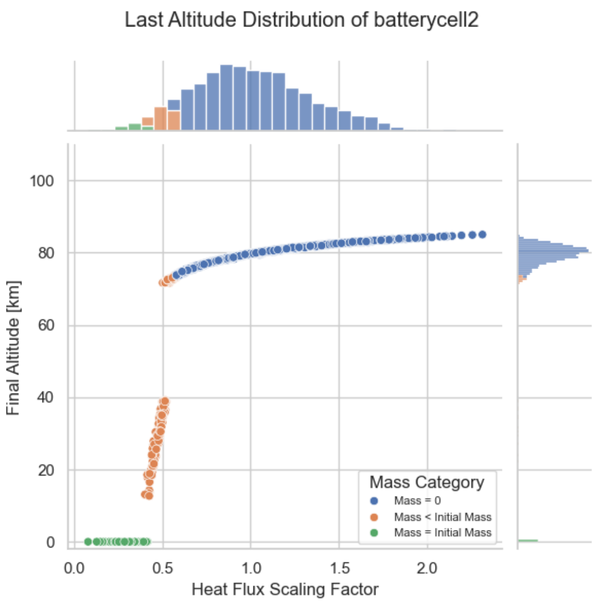

Figure 6: Scatter plot of the battery cell shows a saturation curve indicated by mainly blue data points that equal complete demise. Some data points show surviving of the component indicated by green and orange data points.

The colouring of the plots illustrates that a threshold is achieved at a point where the data points transition from following a saturation curve to a linear regime with orange data points. Most runs with scaling factors above this threshold result in complete demise, indicated by blue-coloured data points, while those below the threshold are shown in orange and green data points. This indicates that the component does not fully demise or even not demise at all but instead tapers off to a $15\,\mathrm{J}$ threshold while still maintaining some mass as, at this point, the energy is reduced by deceleration due to the component's atmospheric drag increasing as the altitude decreases. These fragments will reach the ground but are not considered for the risk analysis.

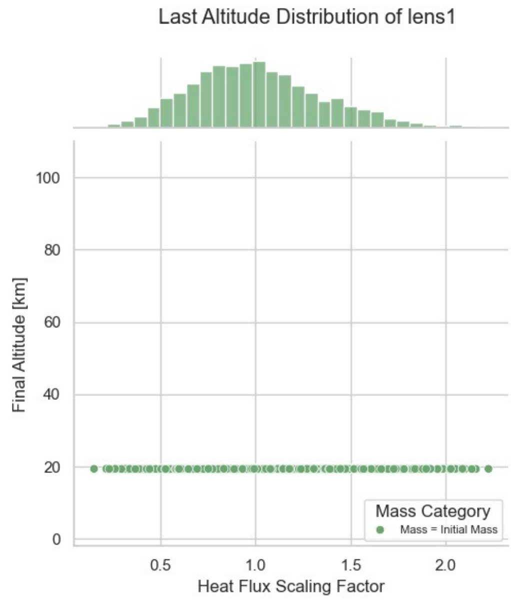

Figure 7: The lens shows no change based on its data points. The green dots indicate no mass loss at all.

The tipping point reached is the radiative equilibrium, meaning the heat flux is equal to the radiated heat of this object [21]. The more the heat flux is reduced, the lower the temperature and the more the component survives, eventually reaching a point where the heat flux is not even causing demise, and the component survives entirely, as indicated by the green data points.
This behaviour can be observed in almost every component's demise behaviour except the lenses of the MeSHCam shown in Fig. 7. It appears that the heat flux has no effect, as the melting temperature is so high that even an increase in heat flux does not lead to a change in the uncritical altitude, where the lens (modelled with drama-SiC) does not demise at all, indicated by the green data points. Its range of last altitudes equals $\Delta_{\mathrm{Lens}} = 0.080\,\mathrm{km}$, which might be due to numerical effects of DRAMA and the parent component being the MeSHCam housing out of aluminium having different scaling factors applied and, therefore, the lenses are released at a different altitude and thus are also affected by a velocity change. So, the effect of the heat flux on the lens with its high melting temperature is negligible.
In most cases, the battery cell demises at an altitude of around $80\,\mathrm{km}$ which equals the DRAMA simulation re-

sult with no uncertainties applied. It reaches a radiative equilibrium at around $72\,\mathrm{km}$. In some cases, the battery cell survives and reaches the ground, which are marked as green dots. The altitude range of the battery cell equals around $\Delta_{\text{Battery cell}} = 84\,\mathrm{km}$. It appears that some orange data points in the battery cell scatter plot remain at higher altitudes, which is due to the step sizes taken for the demise computation. Before the material can completely demise, it already reaches its $15\,\mathrm{J}$ threshold. In reality, the battery cell would likely continue to demise beyond this point, but the simulation stops tracking it once the energy falls below the threshold due to step changes.
It can be concluded that the heat flux uncertainty significantly impacts the demise behaviour of the satellite. However, the heat flux might not affect components with a significant melting temperature, as such components show no demise and have relatively small last altitude ranges.

Drag Uncertainty:
Drag decreases the velocity significantly. Therefore, the $15\,\mathrm{J}$ threshold can be reached quickly. The main driver for heating is the velocity, which is why the final altitude decreases as the drag increases in the higher altitude regions of the main demise area. The components reach a lower altitude as they are slightly slowed down. This effect can be seen if the data is zoomed-in such as in the battery cell scatter plot in Fig. 9. The landed mass of all components, excluding the lenses, is zero.

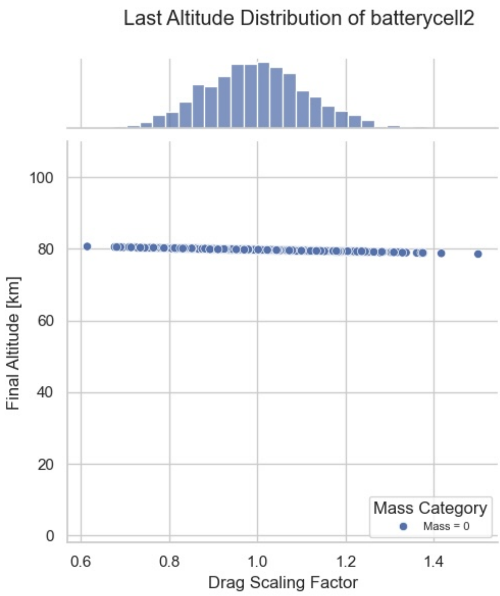

Figure 8: Battery cell scatter plot of drag scaling factor showing that in all cases the component demises.

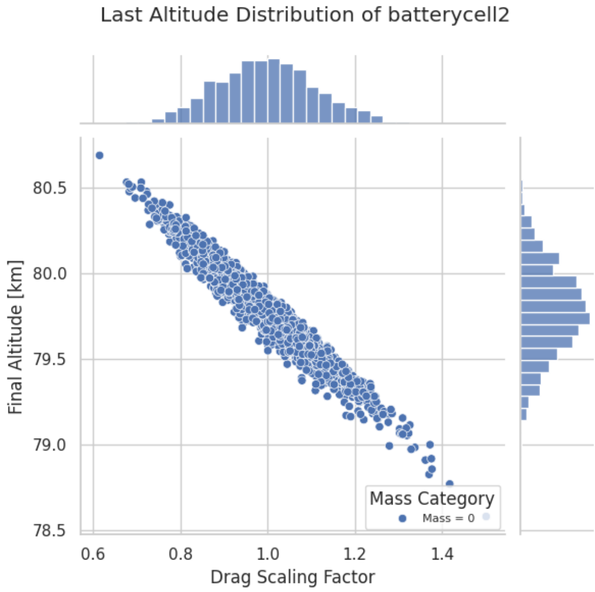

Figure 9: Zoomed-in data indicates the downwards trend with higher scaling factor of the drag

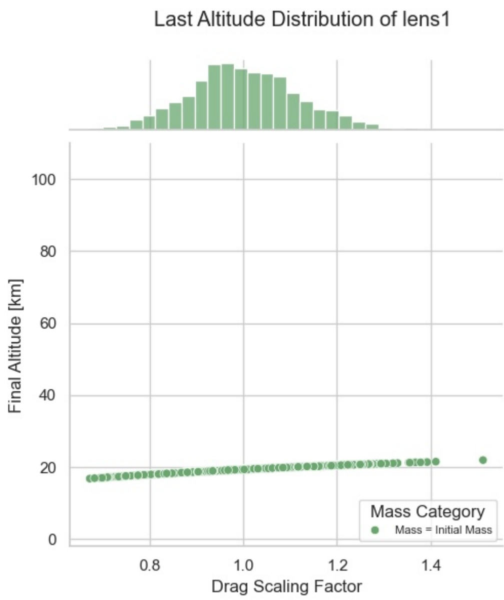

Figure 10: The Lens shows higher last altitudes with increasing scaling factor.

All other components' range of their last altitude is lower than those of the lenses. The lens has a range of roughly $\Delta_{\text{Lens}} = 5\,\mathrm{km}$ for the lenses to reach a $15\,\mathrm{J}$ threshold, whilst the other components have a lower range. The lens shows a big influence compared to its behaviour with the heat flux uncertainty applied. While heat flux did not influence the lens due to its high melting temperature, the drag has an effect as this is not related to its material properties but rather its dimension.
The battery cell in Fig. 8 modelled with the drama-A316 steel model has a range of $\Delta_{\text{Battery cell}} = 1\,\mathrm{km}$.

The drag becomes more relevant as the lens descends through the atmosphere, causing it to get less critical at a higher altitude, while it reaches lower altitudes if the drag is lower. The velocity of the component is dependent on the drag. Therefore, the $15\,\mathrm{J}$ threshold is reached with a decreasing velocity, which is the case for an increasing aerodynamic drag.
All components except for the lenses have low sensitivity to drag. They completely demise at high altitudes in all cases, and their last altitude changes only minimally. The lenses exhibit higher sensitivity to drag, but this has only a minor impact on the final outcome, as they become harmless well above the ground in all cases. Their behaviour is dominated by the velocity loss due to drag and, therefore, changing kinetic energy.
Unlike the heat flux plots, no critical flipping point has been reached where components suddenly stop demising. The sensitivity is overall lower than the one of the heat flux.

Mass Uncertainty:
Mass uncertainty is solely applied to the mass and does not scale the component's dimension according to the mass change. The results show that a higher component mass leads to a lower demise altitude. This can be observed in all components modelled with a material with relatively low melting temperature such as the battery cell in Fig. 11 with a final altitude range of $\Delta_{\text{Battery cell}} = 2.5\,\mathrm{km}$.

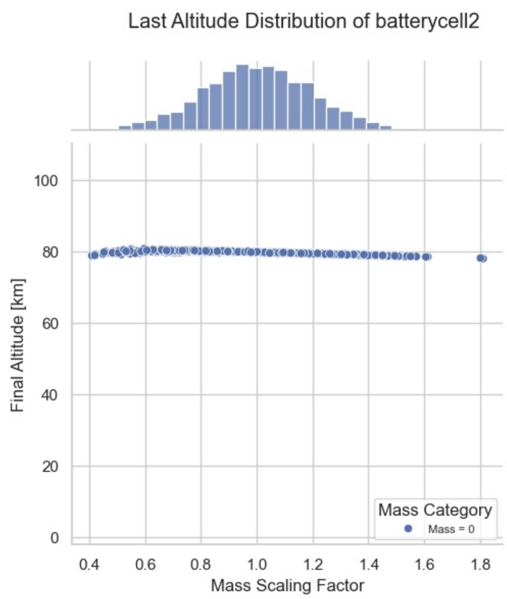

Figure 11: The mass scaling affects the battery cell, showing a clear trend with the scaling factor increasing.

Materials with a higher melting temperature than, e.g. stainless steel, such as titanium, show a different demise behaviour characterised by the BC being more relevant as indicated in Fig. 13. A high BC means that a component retains its high speed for longer, leading to an increased heat flux and thus a higher demise altitude. If the components would also change their size along with the mass, they would demise at an even lower altitude with a smaller mass due to the adapted size-to-mass ratio. Since DRAMA's rigid body assumption maintains a constant geometry while only the mass is scaled, a hypothetical extension that scales the component's size in proportion to the mass would reduce the BC due to an increased drag area.

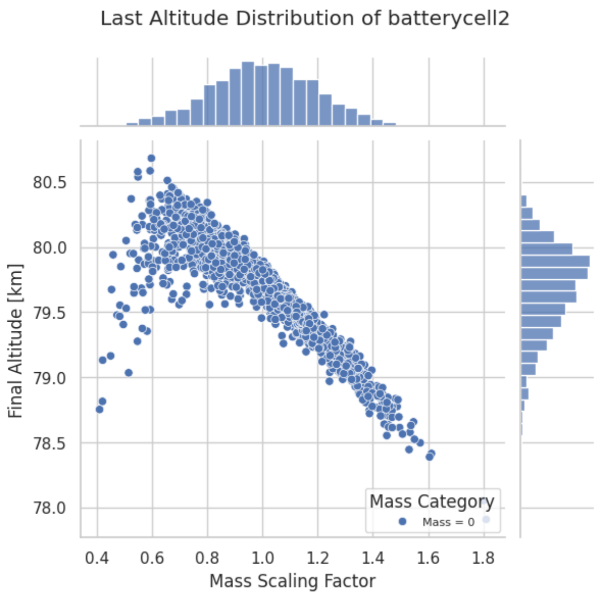

Figure 12: The battery data shows the trend more clearly in a zoomed-in scatter plot.

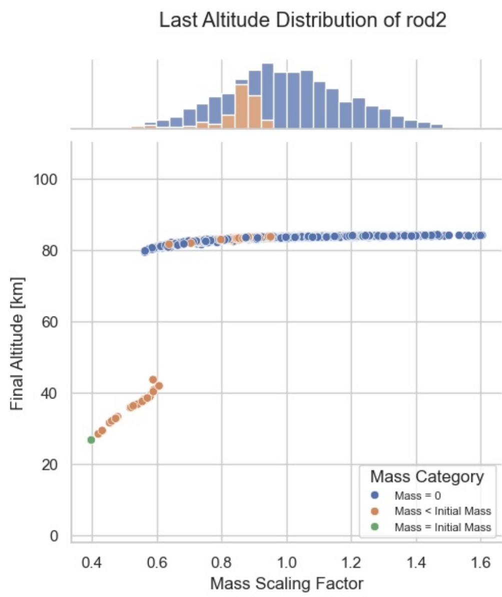

Figure 13: The rod 2 shows that with increasing mass, the altitude increases, and with lower mass, the altitude decreases.

This reduction in BC means that an increase in mass would yield a relatively higher aerodynamic drag, decelerating the component and causing its demise at a lower altitude. Previous drag analyses in Sec. 5.1 support this behaviour, confirming that incorporating size scaling effects and, therefore, drag scaling effects further decrease the demise altitude.
Generally, scattering can be observed due to the BC changing compared to the rest of the spacecraft.
However, the lenses will not demise during re-entry, as their melting temperature will not be reached, making them survive. The higher their mass, the faster their velocity and the higher their kinetic energy. Therefore, heavier lenses become uncritical at lower altitudes as their velocity decreases with decreasing altitudes due to increased drag. This is observable in the lens scatter plot in Fig. 14 where the final altitude range of the lens is given as $\Delta_{\text{Lens}} = 13.5\,\text{km}$. As the mass scaling factor is not being applied to the material properties of the lens, it has a relatively high effect compared to other uncertainties applied, such as the heat flux and the material properties.

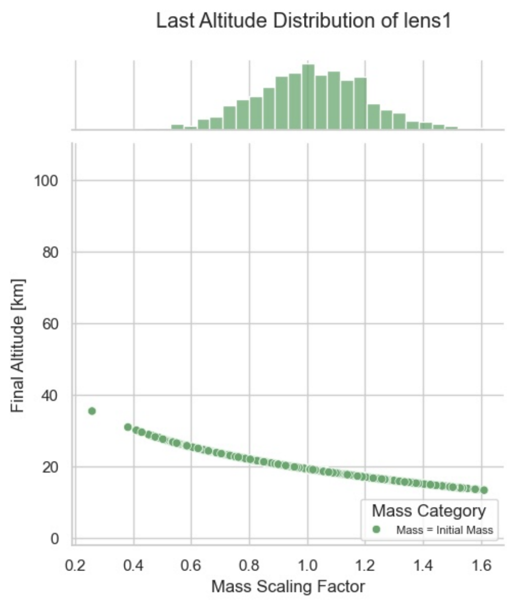

Figure 14: The lens is never surviving, indicated by the green data points. Downward trend as mass is scaled up.

Alloy Melting Temperature Uncertainty:
The change in melting temperature demonstrates the expected behaviour for most alloys, except for the drama-A316 stainless steel material. Typically, setting a higher alloy melting temperature results in the material demising at lower altitudes. The stainless steel material shows a jump around the actual melting temperature in Fig. 15. Other materials show step behaviour in the expected numerical ranges with less than $0.1\,\text{km}$. However, the jump observed in the steel material around $1\,\text{km}$ seems too high to be a numerical step change. To assess whether this behaviour stems from the Python extension or DRAMA itself, the behaviour was replicated with a steel component by Ian Holbrough [23]. The results is the same behaviour, meaning that SESAM generates this issue.

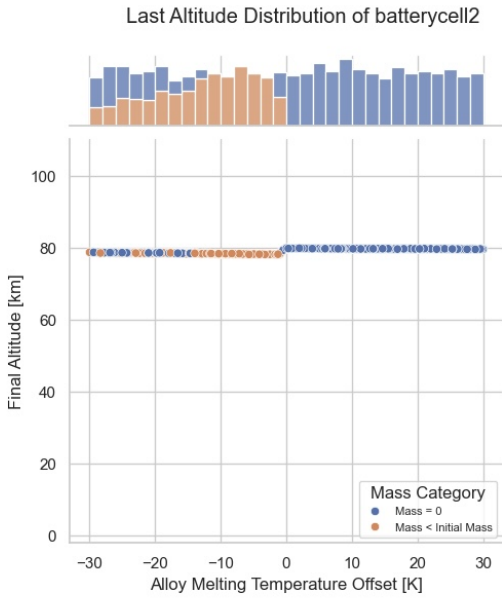

Figure 15: The battery cell shows a jump around its actual melting temperature.

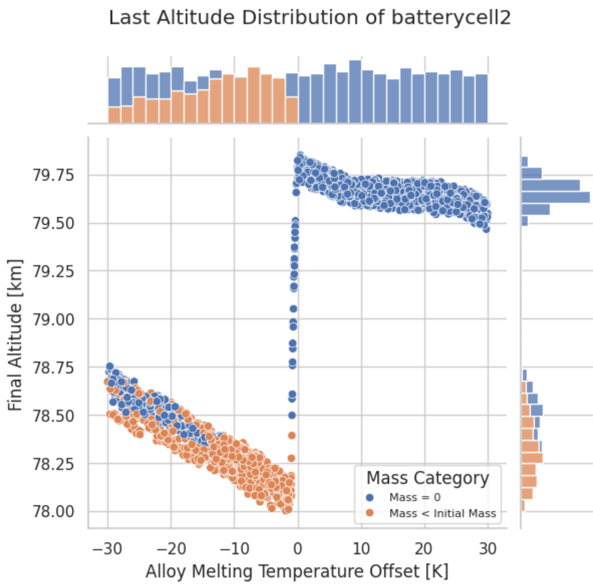

Figure 16: Zoomed-in to the data points of battery cell, the jump is more visible.

As other materials did not show this demise behaviour, this issue is generated by the material definition in the materials.xml data file. The emissivity is defined differently for two different temperatures close to the melting temperature. This means that the emissivity changes as soon as it reaches a temperature of $1664.9\,\text{K}$. The values in the XML for the emissivity are interpolated.

A higher emissivity means that the reflection property changes, whereas the emissivity coefficient 0 is a perfect reflector, and 1 is a perfect emitter. In this case, the emissivity is defined as lower with $\varepsilon_{\text{drama-A316}} = 0.5$ compared to $\varepsilon_{\text{drama-A316}} = 0.85$, meaning that the surface becomes more reflective upon reaching higher temperatures, making a step from $1664.0\,\mathrm{K}$ to $1664.9\,\mathrm{K}$. This step change indicates a high dependency on the emissivity. A small change already affects the demise behaviour about roughly $2\,\mathrm{km}$. Looking at the slope of both arms in Fig. 16, one can see that the left arm, with a lower emissivity coefficient, has a steeper slope than the right one. This shows that the emissivity affects the heat transfer of the component. Meanwhile, the lower emissivity makes the component absorb more heat and, therefore, demise faster. The higher emissivity results in a shallower slope due to the heat being reflected more. Without this emissivity change, the demise points would be continuous. In reality, the emissivity would depend on the nature of the alloy and the formation of an oxide layer during re-entry. Apart from the noticeable jump in components modelled with stainless steel, the overall effect is minimal, so much so that the numerical step sizes become visible. In general, the effect of the alloy melting temperature offset is for the battery cell $\Delta_{\text{Battery cell}} = 0.5\,\mathrm{km}$.
Apart from the jump, no visible change in the altitude ranges is noticeable, in fact, the data points seem to accumulate at the demise altitude, equaling the one of the DRAMA simulations without uncertainties applied. The lenses modelled with drama-SiC show no effect at all, even with slightly lower melting temperatures. The last altitude range for the lens equals $\Delta_{\text{Lens}} = 0.1\,\mathrm{km}$ probably due to release altitude changes through its parent component. The overall effect of the alloy melting temperature is low. This section demonstrates that uncertainties can also originate from software errors, which may initially be overlooked and are sometimes discovered coincidentally, as was the case for the emissivity definition.

Latent Heat Uncertainty:

Latent heat of melting (of fusion) is the energy required to change a material at its melting temperature from a solid material into a liquid. This is because the energy supplied is used to break the intermolecular bonds rather than increasing the kinetic energy of the particles. Therefore, the higher the latent heat of melting is scaled, the lower it will demise as it has a higher temperature change set for the solid-liquid phase change. The effect is negligible, as the plots in Fig. 17 of the battery cell shows that the demise and uncritical altitude remain similar to their initial demise and uncritical altitudes of the DRAMA simulation run with no uncertainties applied. The aforementioned effect becomes slightly visible only when zoomed in. Even numerical step sizes become slightly visible. The range of final altitudes in this case is $\Delta_{\text{Battery cell}} = 0.350\,\mathrm{km}$ for the battery and $\Delta_{\text{Lens}} = 0.100\,\mathrm{km}$ for the lens. Overall, variations in the latent heat of melting have a negligible impact on the overall outcome.

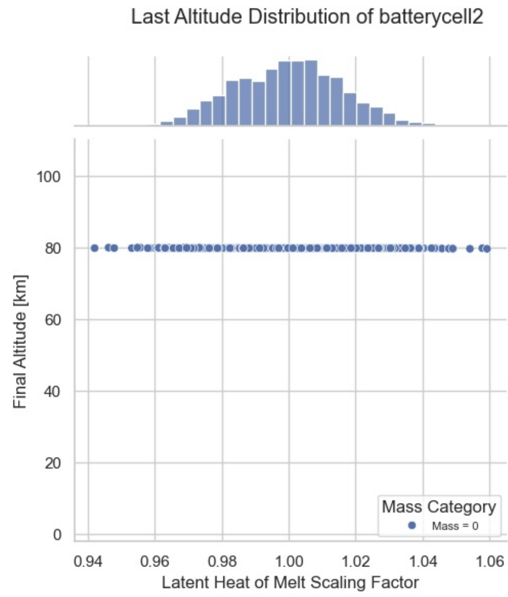

Figure 17: Battery cell showing no visible change.

Heat capacity Uncertainty:

Scaling the capacity of the heat that the material of the component contains affects the component in a negligible way as seen in Fig. 18.

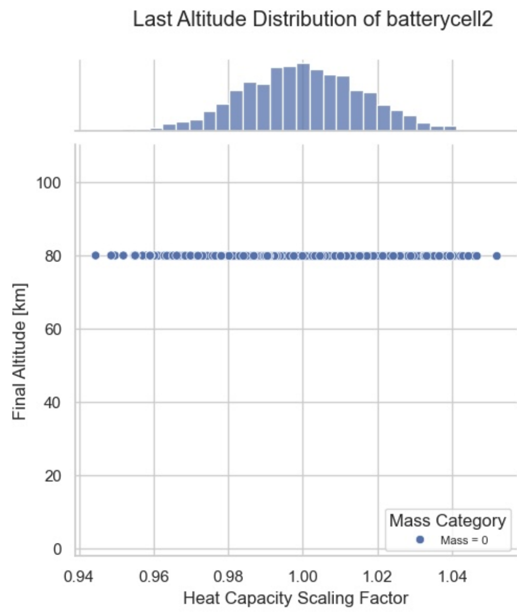

Figure 18: Battery cell shows no visible change in altitude.

The effect is so small that numeric step sizes induced by DRAMA are visible when zooming in on the scale. The increase in heat capacity causes the battery cell to store more heat and, therefore, demise at a slightly lower altitude. The range of the final demise altitude of the battery cell is $\Delta_{\text{Battery cell}} = 0.170\,\text{km}$. The scatter of the data points is higher for nested components compared to those located outside the spacecraft, such as the solar panels, which are exposed from the beginning of the re-entry. However, this scatter is negligible, as it only results in a variation of a few tens of meters. The lenses do not demise and reach the kinetic energy threshold. The Lens is distributed over a last altitude range of $\Delta_{\text{Lens}} = 0.07\,\text{km}$. The change in heat capacity does not affect the lenses, as the range Δ_{Lens} is likely due to a release altitude change induced by its parent component.

Oxidised Emissivity Uncertainty:
With the currently used material definition, no emissivity change was present, as the materials defined in the XML are not configured to change the properties of the oxide formation. This results in no change in the components' demise behaviour, with an altitude range for all components of $\Delta_{all} = 0\,\text{km}$. As every plot looks the same and provides no further information, there was no need to showcase additional plots. However, it was observed that a faulty entry in the emissivity definition for the stainless steel component resulted in a sudden jump behaviour. This indicates that oxidation occurring on the alloy's surface during re-entry impacts emissivity due to the formation of an oxide layer. Further investigation into this effect is recommended.

5.2. Comparison

The summarised Tab. 4 below should give an overview on the altitude ranges of the battery cell and the lens within each uncertainty applied:

Table 4: Comparison of altitude range distribution of the last altitude of the battery cell and the lens.

Parameter	Battery Cell [km]	Lens [km]
Heat Flux	84	0.08
Drag	1	5
Mass	2.5	13.5
Alloy Melting Temp	0.5	0.1
Latent Heat	0.35	0.1
Heat Capacity	0.17	0.07
Oxidised Emissivity	0	0

This table clearly indicates that the heat flux has the highest effect especially on components that are not modelled with materials that remain nearly unaffected by the heat flux such as the drama-SiC material model. In this case the components are more affected by uncertainties regarding their mass and atmospheric drag due to their dimensions. Material uncertainties have an overall low effect on the distribution of the altitudes.

5.3. Risk Results

Only the heat flux uncertainty significantly impacted the casualty risk generation. All other uncertainties did not trigger SERAM to compute a casualty risk, as all surviving fragments did not exceed the $15\,\text{J}$ threshold. Therefore, a detailed look into the risk evaluation with the heat flux uncertainty applied computed by SERAM was taken. The result of 2343 successful runs is 199 runs in which a casualty risk was calculated. The total casualty risk and impact mass values are extracted from the 199 risk output folders generated by SERAM. Only in five cases out of these 199 casualty risk calculations, the casualty risk of 10^{-4} is exceeded. Connections are likely not broken apart, and parent components are not releasing the children due to low heat flux, which leads to bigger and heavier compounds reaching the ground, posing a higher risk. However, it should be noted that while the heat flux uncertainty causes the most significant variation in the output parameters, it only results in a considerable casualty risk in a minority of cases where the lowest scaling factor is applied for this CubeSat. It needs to be assessed by the engineer if actions need to be taken. CubeSats pose low risks as most of the components usually demise fully or are too small to pose a risk. However, for larger platforms, applying uncertainties in risk estimation is more critical, as uncertainties can influence whether certain components survive re-entry and potentially pose a hazard.

6. CONCLUSION

Demise verification is essential to ensure spacecraft comply with casualty risk requirements during re-entry. However, both the verification process (including the modelling by an engineer) and re-entry itself involve significant uncertainties that must be addressed using statistical analyses. Previous studies like PADRE and a master's thesis [3, 2, 5] highlighted the influence of specific parameters on demise predictions.
This study assessed various uncertainties using a simulation toolchain based on SARA with pyDRAMA and a Monte Carlo approach. The results show that uncertainties in aerothermodynamic heating have the most significant effect on demise behaviour, followed by drag and mass. Material uncertainties (e.g. melting temperature, latent heat, heat capacity) had less influence, primarily affecting ablation. However, emissivity changes, particularly in steel, suggest this property may play a larger role than assumed.
Despite these uncertainties, the CubeSat SOURCE remains mainly compliant with casualty risk thresholds in most scenarios. Even with extreme parameter values, only five cases slightly exceeded the limit, and key components like lenses dissipated energy below the critical $15\,\text{J}$ threshold.
Improved material models are needed, as current datasets lack accuracy and had to be substituted. The ESTIMATE database [14] and a potential wind tunnel mode in

DRAMA could help reduce modelling uncertainty. While simulations and ground tests provide valuable insights, in-flight data is essential for validation and model refinement.

To improve the reliability of demise predictions, standardised modelling practices should be implemented [20]. Overall, better data, improved tools, and harmonised processes are key to advancing re-entry safety and spacecraft demisability verification.

ACKNOWLEDGMENTS

Thanks to Martin and Daniel from the Institute of Space Systems, and Marco from the Clean Space Office for being my supervisors. Additionally, I want to thank the Clean Space Team at ESA for making this study possible. Thanks to Daniele, Stijn, and Ian for always being open to my questions.

REFERENCES

1. Ahamed, I., Kaiser, C., Galla, D., Gebhard, K., Liegibel, M., O'Donohue, M., Haufe, P., Hoffmann, P., Jarothe, T., Lips, T., Klinkner, S. & Herdrich, G. Investigation of the Demise Behaviour of Critical CubeSat Components in a Plasma Wind Tunnel. *75th International Astronautical Congress (IAC)*. pp. 1-15 (2024,10)
2. Beck, J., Holbrough, I., Merrifield, J., Bianchi, S., Briot, D., Spel, M., Minisci, E., Omaly, P. & Lemmens, S. PADRE: Probabilistic Assessment of Destructive Re-entry. *Proceedings Of The 5th International Space Debris Re-entry Workshop*. 1 pp. n/a (2020), `https://conference.sdo.esoc.esa.int/proceedings/isdrw05/paper/8/isdrw05-paper8.pdf`
3. Beck, J., Holbrough, I., Merrifield, J. & Lemmens, S. Probabilistic Comparison of Destructive Re-entry Tools. *Proceedings Of The 8th European Conference On Space Debris*. (2021,4), `https://conference.sdo.esoc.esa.int/proceedings/sdc8/paper/279/SDC8-paper279.pdf`
4. Beck, J., Holbrough, I., Lemmens, S. & Virgili, B. Re-Entry Modelling Procedure. (Belstead Research Ltd.,2021,12), `https://sdup.esoc.esa.int/drama/`
5. Callegaro, E. Stochastic Assessment of Destructive Re-entry for LEO Spacecraft. (Cranfield University,2024), Master's thesis
6. Galla, D., Kaiser, C., Haufe, P., Hoffmann, P., O'Donohue, M., Hufgard, F., Dürnhofer, C., Pagan, A., Löhle, S., Herdrich, G. & Klinkner, S. Demise Instrumentation Verification of the CubeSat SOURCE with End-to-End Plasma Wind Tunnel Experiments. *34th International Symposium On Space Technology And Science (ISTS)*. (2023,6), `https://www.researchgate.net/publication/377326947`
7. Demke, M., Haufe, P., Kaiser, C., Zietz, M. & Waizenegger, K. Space Debris Mitigation Report. (KSat e.V.,2023,12)
8. ESA Space Debris Mitigation Working Group ESA Space Debris Mitigation Compliance Verification Guidelines. (ESA,2023,2), `https://sdup.esoc.esa.int/documents/download/ESSB-HB-U-002-Issue214February2023.pdf`
9. ESA Space Debris Office ESA'S Annual Space Environment Report. (ESA,2024), `https://www.esa.int/Space_Safety/Space_Debris/ESA_Space_Environment_Report_2024`
10. ESA DRAMA 3 (Debris Risk Assessment and Mitigation Analysis) Overview and Status. *7th International Conference On Astrodynamics Tools And Techniques (ICATT)*. (2018,11), `https://indico.esa.int/event/224/contributions/3879/attachments/3169/3909/20181108_7ICATT_DRAMA3_SL.pdf`
11. ESA DRAMA Python Package Documentation. (2024), `https://sdup.esoc.esa.int/drama/python_package_docs/index.html`
12. European Space Operations Centre (ESOC) Design for Demise Verification Guidelines. (ESA,2024), `https://sdup.esoc.esa.int/documents/download/Design-for-Demise-Verification-Guidelines-v1.pdf`
13. ESA Space Debris Mitigation Working Group Technical requirements specification. (ESA,2023)
14. ESA ESTIMATE: ESA's Space Debris Mitigation Analysis Tool. (2024), `https://estimate.sdo.esoc.esa.int`
15. ESA Space Debris Office Recovered Debris. (2024), `https://reentry.esoc.esa.int/home/recovereddebris`
16. ESA ESA Re-entry Safety Requirements. (2017), `https://technology.esa.int/upload/media/50K9kQ_6405b2d97d6ec.pdf`
17. ESA Reentry and collision avoidance. (2025), `https://www.esa.int/Space_Safety/Space_Debris/Reentry_and_collision_avoidance`
18. ESA 6th International Space Debris Re-Entry Workshop. (ESA,2025,1), `https://indico.esa.int/event/549/`
19. ESA SDUP (Space Debris User Portal). (2024), `https://sdup.esoc.esa.int/`
20. ESA Space Debris Risk Assessment and Mitigation Analysis Workshop 2025. (2025,3), `https://indico.esa.int/event/545/,WorkshopheldatESA/ESOC,Darmstadt,Germany`
21. Fritsche, B., Lips, T. & Koppenwallner, G. Analytical and numerical re-entry analysis of simple-shaped objects. *Acta Astronautica*. 60 pp. 737-751 (2007)

22. Harris, M. Why satellite mega-constellations are a massive threat to safety in space. (MIT Technology Review,2019,3), https://www.technologyreview.com/2019/03/29/136268/why-satellite-mega-constellations-are-a-massive-threat-to-safety-in-space/

23. Holbrough, I. Personal Communication during the DRAMA Space Debris Risk Assessment and Analysis Workshop.

24. Holbrough, I. Personal email communication with Ian Holbrough. (2024,9)

25. Hook, C., Wright, E., Byers, M. & Boley, A. Uncontrolled reentries of space objects and aviation safety. *Acta Astronautica*. 222 pp. 69-80 (2024)

26. Hyperschall Technologie Göttingen GmbH Final Report: Upgrade of DRAMA's Spacecraft Entry Survival Analysis Codes. (ESA,2019), https://sdup.esoc.esa.int/drama/downloads/documentation/DRAMA-3.0.0-Final-Report.pdf

27. Kanzler, R., Lips, T., Fritsche, B., Breslau, A., Bonetti, D., Fuentes, I., Letterio, F., Miguel, G., Arnao, G., Palomo, P., Parigini, C., Bunte, K., Miller, A., Farahvashi, E., Garms, C., Lorenz, J., Kebschull, C., Funke, Q. & Lemmens, S. DRAMA's Spacecraft Entry Survival Analysis Codes. *Proceedings Of The ESA-ECSL Space Debris Regulation, Standards, And Tools Workshop*. (2019), https://conference.sdo.esoc.esa.int/proceedings/ecsl19/paper/17

28. Karahan, B., *Example scripts for performing Monte Carlo uncertainty analyses using SARA, 2025. https://debris-forum.sdo.esoc.esa.int/t/example-scripts-for-performing-monte-carlo-uncertainty-analyses-using-sara/534.*

29. *Kopacz, J., Herschitz, R. & Roney, J. Small satellites an overview and assessment.* Acta Astronautica. *170 pp. 93-105 (2020)*

30. *KSat e.V. SOURCE Project Renderings. (2025), https://cloud.ksat-stuttgart.de/index.php/apps/files/files/758680?dir=/SOURCE/90__PR_%26_Media_%28Public_Relations%29/05__Renderings/aktuell*

31. *Looten, A. Design for demise applied to spacecraft structural panels and experiments for ClearSpace One platform. (EPFL,2024)*

32. *NASA, Handbook for Limiting Orbital Debris. NASA Handbook 8719.14, Washington, DC 20546, 2008. https://standards.nasa.gov/sites/default/files/standards/NASA/Baseline/1/nasa-hdbk-871914_baseline_with_change_1.pdf*

33. *National Oceanic and Atmospheric Administration (NOAA) Layers of the Atmosphere. (2024), https://www.noaa.gov/jetstream/atmosphere/layers-of-atmosphere*

34. *Pardini, C. & Anselmo, L. The risk of casualties from the uncontrolled re-entry of spacecraft and orbital stages.* Journal Of Space Safety Engineering. *11, 181-191 (2024)*

35. *Park, S., Mischler, S. & Leyland, P. Re-entry analysis of critical components and materials for design-for-demise techniques.* Advances In Space Research. *68, 1-24 (2021)*

36. *Persis, C. & Lemmens, S. An Overview of the Destructive Re-Entry Analysis Tools Available in Europe: State of the Art, Latest Advances, and Open Points.* Journal Of Space Safety Engineering. *11 pp. 35-43 (2024,1), https://www.sciencedirect.com/science/article/pii/S2468896723001301*

37. *SCARAB AUTODOC System Re-Entry Analysis Documentation. (Hyperschall Technologie Göttingen GmbH,2023,8)*

38. *United Nations Office for Outer Space Affairs (UNOOSA) Convention on International Liability for Damage Caused by Space Objects. (2024), https://www.unoosa.org/oosa/en/ourwork/spacelaw/treaties/liability-convention.html#:~:text=A%20launching%20State%20shall%20be,earth%20or%20to%20aircraft%20flight.*

39. *Velarde, C., Bewick, C., Fittock, M. & Carná, S. Early Phase Re-entry Analysis of ESA Earth Observation Missions to Advance Satellite Design Choices.* Proceedings Of The 8th European Conference On Space Debris. *(2021), https://conference.sdo.esoc.esa.int/proceedings/sdc8/paper/201/SDC8-paper201.pdf*